Integrating GaAs, Si, and Dye-Sensitized Solar Cells in Multijunction Devices and Probing Harsh Condition Behavior

Hammad Cheema, † Jonathon Watson, † and Jared H. Delcamp*

Coulter Hall, Department of Chemistry and Biochemistry, University of Mississippi, University, MS, 38677, United States.

KEYWORDS. dye-sensitized solar cells, SSM-DSCs, multijunction solar cells, renewable energy, integrating technologies

ABSTRACT. Mechanically stacked single illuminated area sequential series multijunction dyesensitized solar cells (SSM-DSCs) were fabricated with varying bottom devices including DSC, silicon (Si), and gallium arsenide (GaAs). Use of near-infrared (>750 nm) photons for conversion to electricity is probed for each of the three technologies. The effect of using these photons on multijunction device power conversion efficiencies is investigated with a three subcell SSM-DSC design where the top and middle subcells were DSC devices with D35 and B11 sensitizers, respectively. The power conversion efficiencies were found to follow the order: DSC/DSC/GaAs > DSC/DSC/DSC > DSC/DSC/Si. Low light conditions were examined for the third subcell technologies as independent solar cells to understand the effects of receiving low light intensity as part of a multijunction system. GaAs and DSC as bottom devices both demonstrated a superior response under filtered or reduced illumination to that of Si in these studies.

Introduction.

Solar cells are developing into a reliable and wide spread sustainable energy source. 1-2 The ability of solar cells to generate electricity is an attractive and sustainable option due to the renewable nature, mobile accessibility, options for building integration, uses under varied environments, and cost advantages of the technology.²⁻⁵ Among the most studied photovoltaic (PV) materials in the solar cell field are silicon (Si), gallium arsenide (GaAs), and dye-sensitized solar cells (DSCs).^{2, 6} Si solar cells are unique as they are able to efficiently harvest low energy photons near 1200 nm, and they have approached the Shockley-Queisser limit (~33%) for power conversion efficiency from a single junction PV device (Figure 1). Si PVs also hold approximately 90% of the PV market share today.² Si PVs generally yield high photocurrents with modest photovoltages (~500 mV).² GaAs PVs have also approached the Shockley-Queisser limit while retaining high photovoltages (~800 mV) but often require higher energy photons (<900 nm).8 DSCs have emerged as a commercially viable, mass producible technology owing to solution processability, production possibilities such as roll-to-roll, an aesthetically pleasing variety of color options, low light performance, and the use of precious metal free materials.⁹⁻¹⁵ DSCs generally use high energy photons most efficiently in terms of photovoltage outputs (near 1.5 V possible) with limited examples using photons efficiently beyond 800 nm. 16-20 Combining these materials into a multijunction system is an attractive way to probe leveraging the high performances of each technology for a particular metric into a higher overall efficiency device (Figure 2).

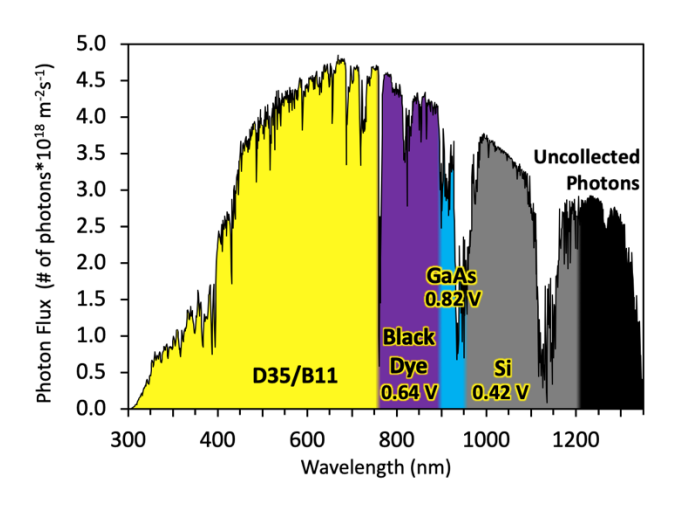


Figure 1. Spectral signature and photovoltage output for each subcell type.

DSCs are attractive technologies for combining in tandem and mechanically stacked multijunction systems as the top and middle subcells (stand-alone solar cells mechanically stacked and wired together to form a multijunction device) since the transparency of DSC subcells can be readily controlled by component selection and amounts used in the subcell.²⁰⁻³⁰ Additionally, DSCs can provide high voltages for series wired devices to boost the overall efficiency of the system.^{18-19, 31} The bottom subcell can then be comprised of any solar cell technology that can use photons at lower energy than the DSC subcells before it. Since DSCs commonly use higher energy photons, lower energy photons are readily available to a bottom subcell made of **Si** or **GaAs** which does not need to be transparent (Figure 2). While tandem devices (specifically 2 subcells total) are well known in the literature combining 1 DSC subcell with 1 inorganic subcell, the use of inorganic subcells in SSM systems with 2 DSC subcells has not been explored to the best of our knowledge.^{20-21, 27-30}

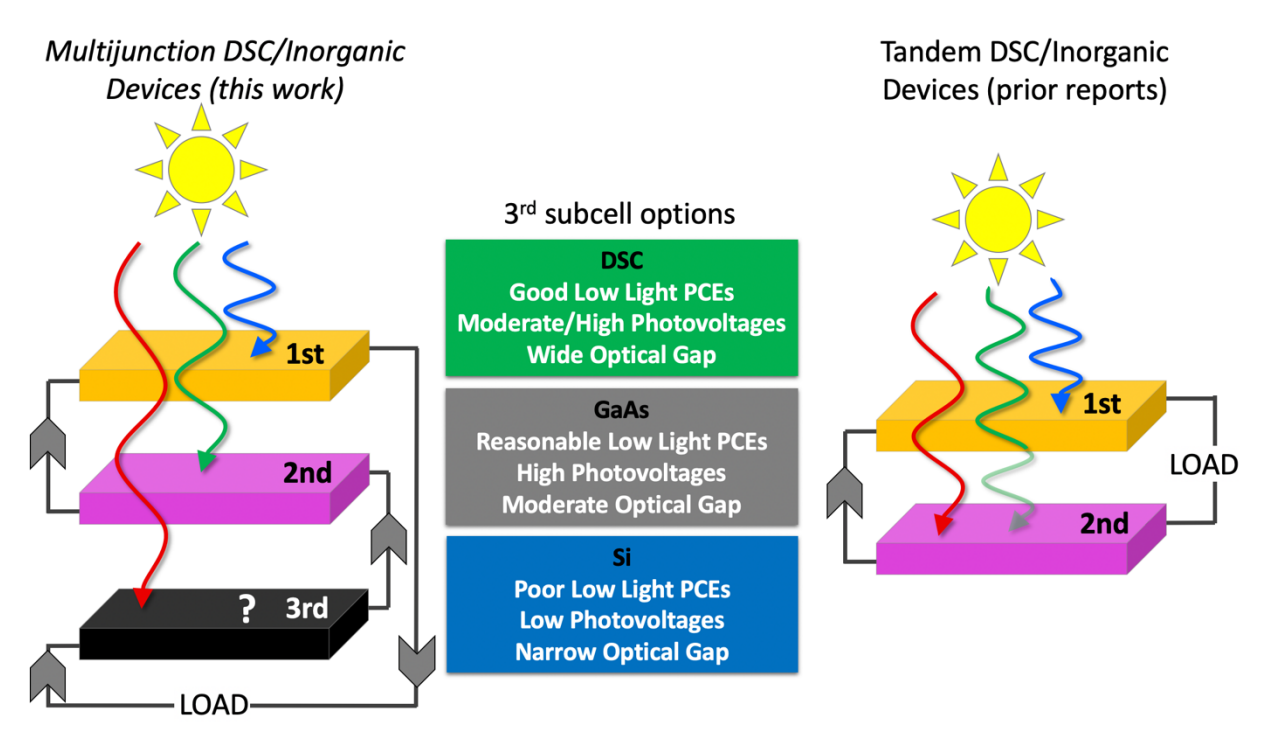


Figure 2. Illustrations of multijunction (left, 6-terminal with series wiring) versus tandem (right, 4-terminal with series wiring) systems with typical attributes listed for the third subcell options.

Results and Discussion.

Organic dye **D35** was selected for the first DSC subcell based on the incident photon-to-current conversion efficiency (IPCE or external quantum efficiency (EQE) as is used in some photovoltaic areas) onset of 600 nm and the high photovoltages (>1000 mV) obtainable with this dye from higher energy photons in the solar spectrum (Figure 3).³²⁻³³ Ruthenium based dye **B11** was selected as the second DSC subcell dye given a

Figure 3. Chemical structures of sensitizers and cobalt redox shuttles employed in this study.

broad IPCE spectrum that reaches 800 nm while retaining a good photovoltage of ~700 mV (Figure 4).³³⁻³⁴ Alternatively, **MK-2** is a highly stable dye (discussion below) that shows a similar IPCE spectral response and can be used in all organic dye based devices in place of **B11** in SSM-DSC devices.³⁵ **D35** and **B11** (or **MK2**) allow for complementary spectral use with both dyes collecting photons over 200 nm ranges (400-600 nm and 600-800 nm, respectively). Recently, **AP25** has been used as a bottom DSC subcell in a three-subcell SSM-DSC device.³⁶ This sensitizer is attractive as an organic sensitizer given the record high photocurrent observed in a DSC device based on organic dyes using **AP25** co-sensitized with **D35**. Additionally, ruthenium-based **Black Dye** has been used in a SSM-DSC device giving the highest reported 3 subcell SSM-DSC power conversion efficiency (PCE >11%) to date.^{33, 37-38} These two examples serve as state-of-the-art all-DSC benchmarking systems for the SSM-DSC/inorganic mixed systems. **Si** PVs harvest photons relatively far into the NIR spectrum (near 1200 nm) which complements the IPCE spectral response of **D35** and **B11** (Figure 4). The broad IPCE response of **Si** PVs is attractive for replacing bottom DSC subcells in SSM-DSC devices. **GaAs** solar cells offer a close to optimal bandgap (E₈

= 1.42 eV) for a single junction device based on the Shockley-Queisser limit with good photovoltages based on this bandgap.² The performance of each configuration (1) SSM-DSC, (2) SSM-DSC/Si, and (3) SSM-DSC/GaAs are all compared herein with a 6-terminal, series wired design. Each subcell of the multijunction device is a stand-alone solar cell independently fabricated and mechanically stacked with the terminals of the subcells wired in series.

First, the individual solar cell devices intended for use as bottom subcell devices in an SSM-DSC configuration were analyzed (Figure 4, Table 1). The PCE values were calculated according to the equation PCE = $(J_{sc} \times V_{oc} \times FF)/I_0$, where J_{sc} is the short-circuit current density, $V_{\rm oc}$ is the open-circuit voltage, FF is the fill factor, and I_0 is the intensity of the incident light (1 sun, air mass 1.5G, 100 mW/cm², unless otherwise noted). Black Dye and AP25+D35 demonstrate a broader light harvesting ability with a 900 nm absorption onset relative to B11 with an 800 nm absorption onset. An IPCE peak efficiency of >80% was observed for both Black Dye and AP25+D35 based devices. (Figure 4). J_{sc} values of 23.7 mA/cm² with AP25+D35, 20.8 mA/cm² with Black Dve, and 17.5 mA/cm² for B11 were observed (Figure 4). PCEs according to the following trend were observed: **Black Dye** (9.5%) > **B11** (8.5%) > **AP25+D35** (8.3%) (Table 1). Given the inverse relationship of J_{sc} and PCE for Black Dye and AP25+D35 based DSC devices, the relative importance of these two parameters on the SSM-DSC devices can be probed in these studies. Compared to the DSC devices, the **GaAs** PV device used in these studies shows a high J_{sc} of 27.0 mA/cm² with a PCE of 15.9% (Figure 4, Table 1). Si PV devices come with a wide range of performances, and for these studies a device with a very high photocurrent was selected as the third subcell to probe the effects of a high current/low voltage (Si PV) versus a high voltage/low current (GaAs) subcell on multijunction solar cell performance. Photocurrent was observed to be the highest for the Si PV device used in these studies at 53.1 mA/cm² due to its broad IPCE

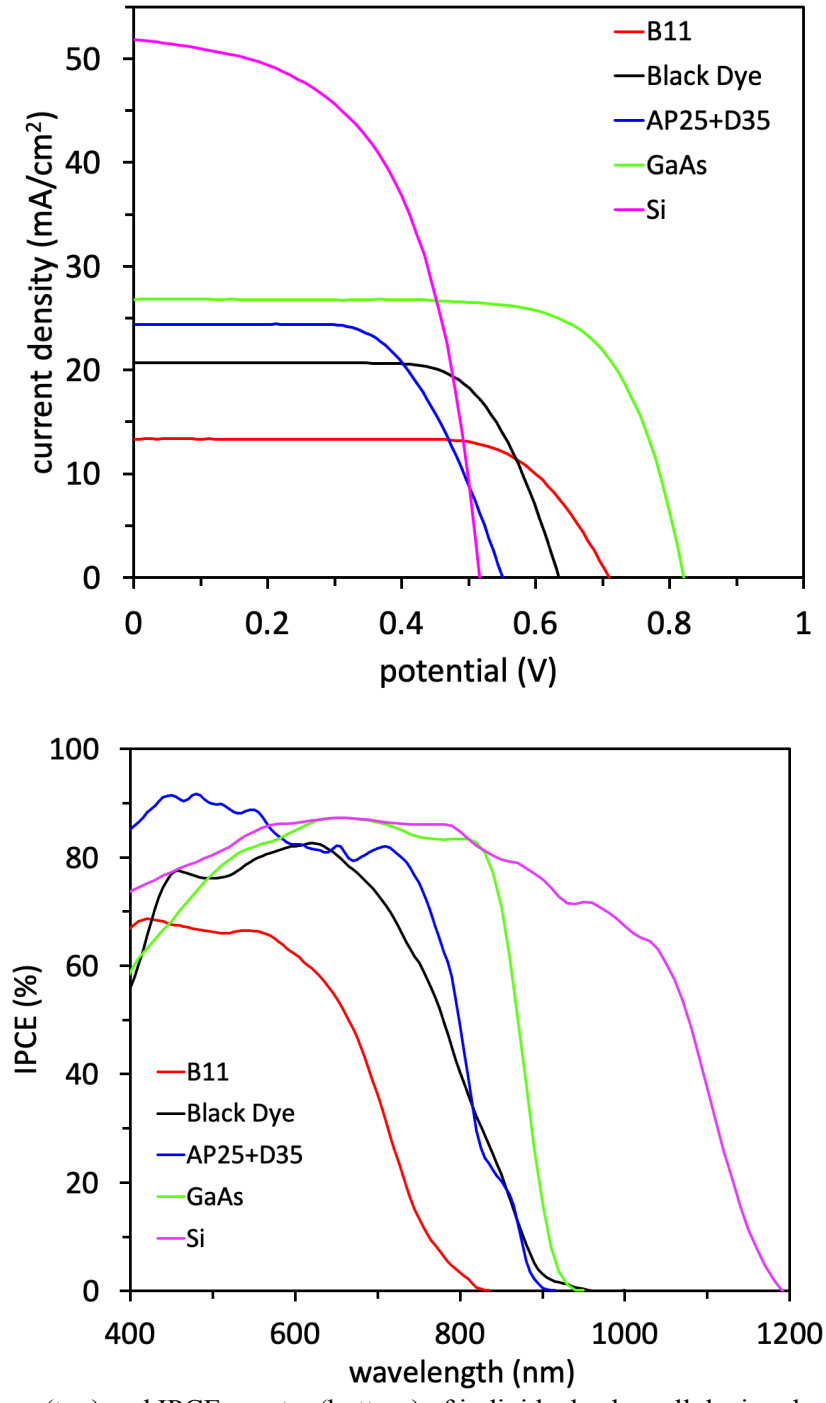


Figure 4. *J-V* curves (top) and IPCE spectra (bottom) of individual solar cell devices based on: DSC (**B11**, **Black Dye**, **AP25+D35**), **GaAs**, and **Si** PV devices.

Table 1. Comparison of PV device performance metrics of individual solar cell devices.

arison of the device performance metrics of marvidual solar cent devices.						
Devices	J_{sc} (mA/cm ²)	V _{oc} (mV)	FF (%)	PCE (%)		
B11 ^a	17.5 ± 1.0	686 ± 10	70 ± 3	8.5 ± 0.2		
Black Dyea	20.8 ± 0.4	644 ± 7	70 ± 1	9.5 ± 0.1		
AP25+D35 ^a	23.7 ± 0.7	570 ± 11	63 ± 1	8.3 ± 0.2		
GaAs	27.0 ± 0.6	824 ± 12	70 ± 3	15.9 ± 0.2		
Si	53.1 ± 1.9	518 ± 4	56 ± 1	16.2 ± 0.8		

^a Device preparation details are located in the experimental section.

response with an overall PCE of (16.2%). Thus, the J_{SC} trend is as follows: Si > GaAs > DSC, and the photovoltage trends are as follows: GaAs > DSC > Si for the devices used in this study. The all DSC-based SSM-DSC devices (D35/B11/B11, D35/B11/Black Dye, D35/B11/AP25+D35 and D35/MK2/AP25+D35) have been previously reported (Figure 5, Table 2).33 In these cases, the SSM-DSC devices resulted in a greater PCE than any single DSC device showing that the collective is greater than the parts for the SSM-DSC only devices (Table 1 and 2). The highest performing SSM-DSC/inorganic PV based device utilizes a D35/B11/GaAs configuration, with an overall PCE of 11.2% (Table 2, Figure 5). The D35/B11/GaAs device performance is lower than the single GaAs solar cell (PCE of 15.9%); however, the D35/B11/GaAs device improves upon the previous literature reported PCE with a mechanically stacked DSC and GaAs device at 7.3%. Notably, the **DSC/DSC/GaAs** configuration was found to have a high V_{oc} of 2.5 V which is sufficient to power PV-electrochemical cell systems. 21-22, 39 The D35/B11/Si SSM-DSC/inorganic device gave an overall PCE of 9.1% (Table 2). Importantly, the SSM-DSC-based systems are straight forward to construct with a simple mechanical stacking of individual singleactive layer devices with a series wiring. The SSM-DSC devices could be made with a high degree of reproducibility via screen printing of the TiO₂ paste layers at varied thicknesses to control

transmittance and absorbance at each active layer. All of the systems studied herein were prepared with error bars typically lower than $\pm 0.2\%$ PCE when electrodes of identical thickness were employed. Selection of active layer thicknesses is the one of the most challenging parameters to control whereas cases arise such as the AP25+D35 subcell-based devices shown in Figure 5. In this case, the photocurrent at the AP25+D35 subcell was lower than that of the first two subcells $(J_{SC} = 6.2 \text{ mA/cm}^2 \text{ versus } 7.0 \text{ and } 6.9 \text{ mA/cm}^2 \text{ for the first and second subcells, respectively}).^{33}$ Theoretically, thinning of the active layer TiO₂ paste at the first two subcells would resolve the mismatched photocurrent between the subcells. However, in practice this would require TiO₂ active layer thickness to be accurately controlled down to ~0.1 µm to eliminate mismatched photocurrent completely. With the screen printing techniques and paste dilution approaches used for this project, the accuracy of active layer thickness seems be limited to about $\pm 0.2 \, \mu m$ which leads to cases where mismatched photocurrent is evident in the J-V curve. The J-V curve shows a shape having "steps" in the region where the current would typically be unchanging with voltage (Figure 5, blue curve between 0.75 and 1.0 V). This presents as a diminished fill factor in the overall PCE equation and a reduced SSM-DSC system photocurrent relative to the stand-alone solar cells measured within the SSM-DSC construct (stand-alone subcells give 7.0/6.9/6.2 mA/cm² for the 1st, 2nd, and 3rd devices while the whole SSM-DSC system gives 6.3 mA/cm²).³³ However, many of the multijunction systems studied show very little mismatch.

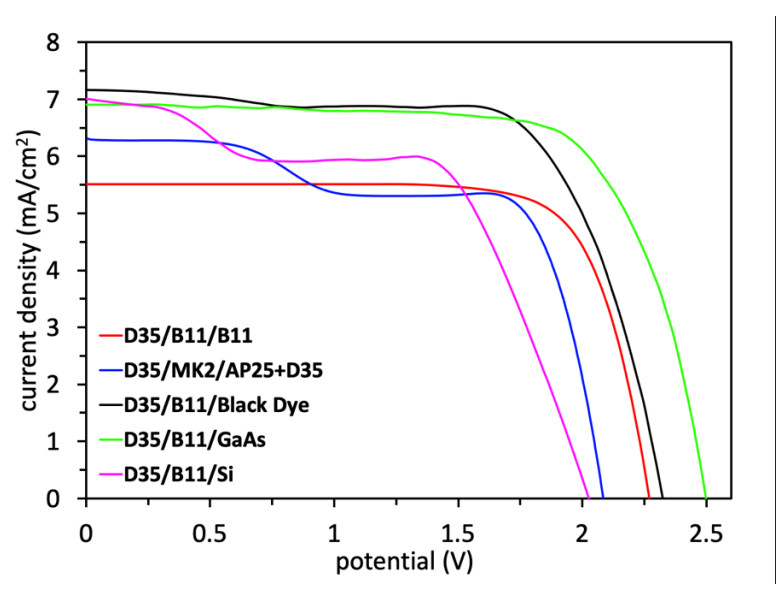


Figure 5. J-V comparison of three subcell SSM-DSCs with the third cell as either a DSC (B11, Black Dye, AP25+D35), GaAs, or Si. The 6-terminal systems are wired in series.

Table 2. Summary of device data for different SSM-DSCs as 6-terminal systems wired in series.

Device ^a	<i>V_{oc}</i> (mV)	J_{sc} (mA/cm ²)	FF (%)	PCE (%)
D35/B11/B11	2281 ± 20	5.5 ± 0.1	71 ± 2	9.3 ± 0.1
D35/B11/Black Dye	2299 ± 37	7.1 ± 0.3	67 ± 3	11.1 ± 0.2
D35/B11/AP25+D35	2322 ± 2	5.9 ± 0.1	61 ± 1	8.4 ± 0.0
D35/MK2/AP25+D35	2132 ± 21	6.3 ± 0.4	68 ± 3	9.5 ± 0.5
D35/B11/GaAs	2472 ± 27	6.9 ± 0.3	68 ± 3	11.2 ± 0.1
D35/B11/Si	2063 ± 5	7.0 ± 0.6	64 ± 6	9.1 ± 0.1

^a See SI for device details and assembly protocols. The first four entries literature reported values.³³

The J-V and IPCE responses of the bottom subcells were measured individually within the SSM-DSC and SSM-DSC/inorganic device configurations to better understand how efficiently the final subcells are using the filtered photons arriving at this subcell (Figure 6, Table 3). Among the SSM-DSC devices, the performance of **Black Dye** as a bottom subcell was superior to the other bottom subcells with **B11** and **AP25+D35**. The J_{sc} of **B11** as a bottom device was mainly limited due to its blue-shifted IPCE onset that inhibited light absorption (Figure 6). The lower PCE of

AP25+D35 (2.7%) within the SSM-DSC configuration compared to Black Dye (3.4%) was due to an \sim 50 mV lower V_{oc} value and a 0.5 mA/cm² lower J_{sc} value. Thus, the red-shifted absorption of Black Dye relative to B11 and the higher V_{oc} of Black Dye relative to AP35 + D35 led to DSC only SSM-DSC devices based on Black Dye being the most efficient at converting sunlight to electricity. The performance of GaAs as the bottom subcell was superior to all other solar cell technologies studied here. This is a result of deeper NIR photon use than the DSC devices with an IPCE onset shift of \sim 50 nm (Figures 4 and 6), and a significantly higher V_{oc} than Si by 296 mV as a third subcell in a multijunction device. Notably, Si as the bottom subcell maintained the highest J_{sc} of 17.8 mA/cm² due to its broad IPCE response which indicates use of this device with more red-shifted SSM-DSC device components could be beneficial, although it is noted that in a series wired configuration the Si device would contribute only ~0.4 V to the overall photovoltage of the SSM device (Figure 6, Table 3). Since Si maintains the highest photocurrent under filtered light for all of the bottom subcell SSM devices, it was further studied as the bottom device in a four subcell SSM-DSC/inorganic device where the dyes were chosen to evenly distribute photon absorption among the subcell layers (D35/Y123/Black Dye/Si) and in a DSC/inorganic tandem device (B11/Si) (Figure S3, Tables S1). A PCE of 10.3% is observed for the tandem device, and with the four subcell SSM-DSC device (D35/Y123/Black Dye/Si), the bottom Si cell demonstrated a well-matching photocurrent with other devices in the stack, however, the gain in V_{oc} relative to the three subcell D35/B11/Si multijunction device (2.7 V versus 2.1 V) was offset by a reduction in SSM device photocurrent (4.7 mA/cm² versus 7.0 mA/cm²) resulting in a lower PCE of 8.5% (Tables 2 and S1).

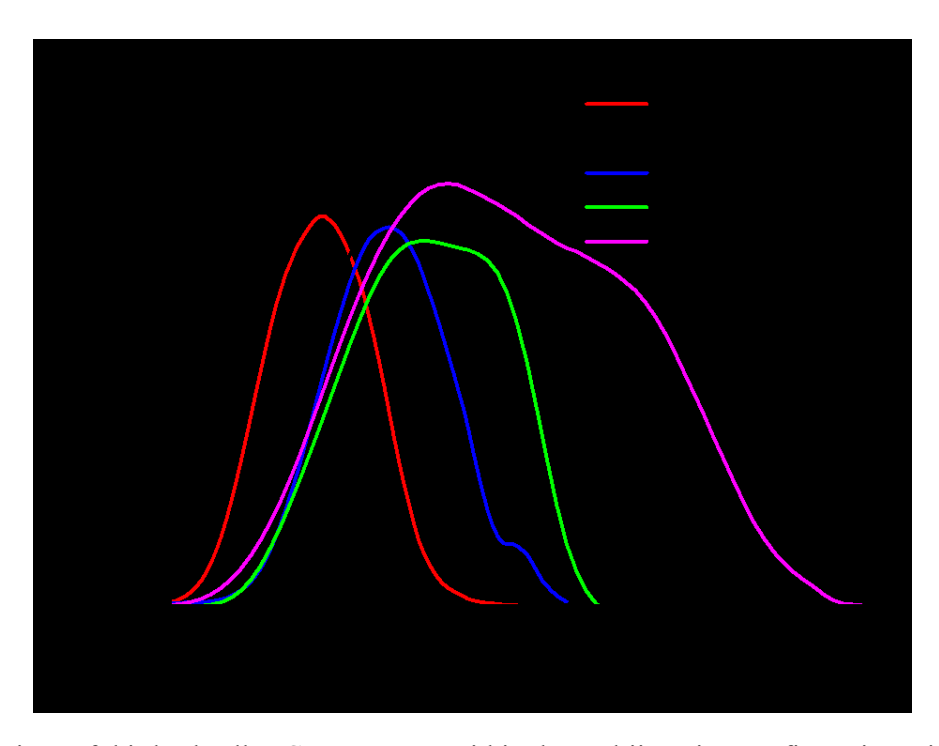


Figure 6. Comparison of third subcell IPCE responses within the multijunction configuration with a **D35** front subcell and a **B11** second subcell. The first two subcells are left as open-circuit photon filters, and the third subcell is measured as a stand-alone solar cell.

Table 3. Summary of third subcell device metrics measured within the SSM-DSC configuration. The first two subcells (**D35** DSC and **B11** DSC) are left as open-circuit photon filters, and the third subcell is measured as a stand-alone solar cell.

Device	Voc (mV)	J_{sc} (mA/cm ²)	FF (%)	PCE (%)
B11	658 ± 7	5.4 ± 0.1	77 ± 1	2.8 ± 0.1
Black Dye	612 ± 3	6.7 ± 0.2	78 ± 1	3.4 ± 0.1
AP25+D35	567 ± 11	6.2 ± 0.1	77 ± 1	2.7 ± 0.1
GaAs	732 ± 4	7.6 ± 0.2	71 ± 1	3.9 ± 0.2
Si	436 ± 2	17.8 ± 0.0	52 ± 1	4.0 ± 0.8

Importantly, PCE values must remain high under reduced light intensities for bottom subcells to operate efficiently in multijunction devices. Thus, each of the bottom subcell devices were removed from the SSM configuration and measured under reduced light intensities (Figure 7, Table S2). DSCs are becoming well-known for operating very efficiently in low-light

environments relative to other solar cell technologies.^{5, 15, 40-41} Interestingly, the AP25+D35 devices show a *substantial increase* in efficiency under low light conditions with a 39% improvement from a PCE value of 6.7% under 1 sun intensity (100 mW/cm²) to 9.3% under 0.1 sun intensity (10 mW/cm²). Black Dye shows a relatively modest 14% PCE improvement in device performance when 1 sun intensity and 0.1 sun intensity are compared. GaAs shows minimal changes in efficiency as sun intensity is diminished from 1 sun to 0.1 sun with only a 5% drop in PCE. An inherent challenge with using Si PVs in higher subcell configurations than 2 subcell devices is apparent as the PCE value drops by 59% as sunlight intensity is reduced from 1 sun to 0.1 sun. These findings indicate that DSCs are an excellent technology for incorporation in multijunction devices if proper chromophores can be found since the devices *improve* in performance at low light significantly compared to no change with GaAs and a dramatic drop with Si PVs.

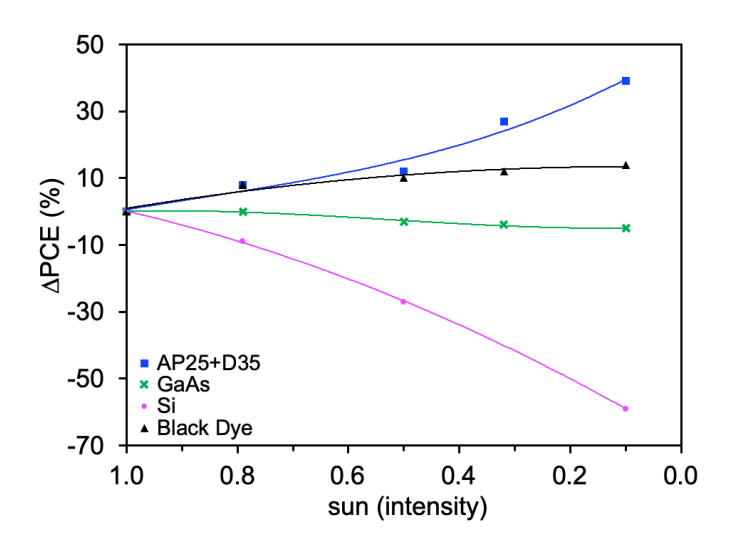


Figure 7. PCE values of **Black Dye**, **AP25+D35**, **GaAs** and **Si** devices as a function of sun intensity. The devices are measured as stand-alone solar cells. Note: A additional **Si** reference cell was measured at a 44% loss of PCE at 0.1 sun intensity relative to 1 sun indicating the PCE-sun intensity trend exists across multiple **Si** devices with a wide 1 sun performances range from 16.2% to 7.4% at 1 sun.

The 3 subcell SSM devices with **Black Dye**, **GaAs**, and **Si** show significant light intensity PCE dependence with improved performances at low light intensities (Figures S6-S8, Table S4). The multijunction devices were all fabricated with similar PCE values near 9% and an increase of PCE up to 11% at 0.1 sun was observed for the **Black Dye** and **GaAs**-based systems (Table S4). This represents a 28% and 15% increase in PCE, respectively. Interestingly, the **Si**-based multijunction device also shows a 5% increase in PCE at 0.1 sun relative to 1 sun. Given the lower performance of **Si** under low light conditions (Figure 7), the increase in PCE suggests the DSC subcells are operating more efficiently at 0.1 sun than 1.0 sun such that the performance loss from the **Si** subcell is offset. To probe this theory, the **D35** and **B11** DSC devices were examined with varied light intensity (Figures S4-S5, Table S3). Both devices show significant increases in performance at 0.1 sun relative to 1.0 sun with increases in PCE of 21% for **D35** and 26% for **B11**. Thus, the DSC subcells both allow adequate photon transmission and an increase in PCE of absorbed photons at low light intensity which gives an increased PCE of the multijunction device at low light intensity (Figure S10).

As an additional evaluate of the practicality of DSC devices in a variety of settings, extreme environmental conditions were probed with three different iodine-based electrolytes (a gel with MeCN and 4% poly(vinylidene fluoride) (PVDF),⁴² EL-HSE, and EL-UHSE, Figure 8).⁴³⁻⁴⁶ EL-HSE and EL-UHSE are commercially available electrolytes with 3-methoxypropiononitirle and ethyl isopropyl sulfone listed as the solvent component, respectively. DSC devices sealed with both Surlyn and a UV curable glue gave initial PCE values of 7.4%, 5.5%, and 3.7% for the gel, EL-HSE, and UL-HSE, respectively. The DSC devices were continuously light soaked at room temperature for 120 hours to show no dramatic changes in PCE (<10 % change in PCE values).

EL-HSE-based devices show a slight decrease in performance while the gel and EL-USE electrolyte-based devices show slight increases in performance. To stress the devices under aggressive conditions, the devices were heated to 120°C and then cooled to -78°C to probe extreme temperature effects. After heating to 120 °C for 4 hours and measuring the device while it was still hot to touch (~50-60°C), both the EL-HSE and EL-UHSE electrolyte devices show a significant *improvement* in the PCE to 6.9% and 5.9% (from 5.5% and 3.7%), respectively. Under the same treatment the gel electrolyte device ceased to function and was not measured further. The EL-HSE and EL-UHSE devices were then allowed to cool to room temperature and submerged in a dry ice acetone bath (-78 °C) for 1 hour. The device performance was then measured while the device was cool (after condensation stopped forming near 0°C) to give a PCE of 6.7% and 5.2% for the EL-HSE and EL-UHSE devices, respectively. This result shows that the performance gained by heating to 120°C is retained even at low temperatures. The devices were then heated to 120 °C for 20 hours to further stress the DSCs. PCE's of 5.4% (EL-HSE) and 3.9% (EL-UHSE) were obtained, which is similar to that observed for the initial devices. PCE values of 4.4% (EL-HSE) and 4.0% (EL-UHSE) were observed after an additional 8 days of continuous light soaking at room temperature. Finally, after heating to 120°C for 20 more hours, the device sealant lost integrity for both systems and the PCE dropped to 1.3% (EL-HSE) and 2.7% (EL-UHSE). These results show the viability of DSCs over a wide range of temperatures (~200°C change) despite using a liquid electrolyte. Notably, UV resins have been found to impart significant stability when used with perovskite white light-emitting diodes that are typically sensitive to ambient conditions.⁴⁷⁻⁴⁹ Device performances were maintained during extreme condition exposure including temperature variation, continuous light soaking, and submersion in organic solvent provided a proper electrolyte and sealant strategy is employed. Thus, the dye and electrolyte components have shown exceptional stability in these systems and high performance under low light conditions (see above) which makes them suitable for use in extreme environments as multijunction solar cell components. Notably, both GaAs and Si PVs are known to dramatically *decrease* in performance as temperatures become elevated (~13% and ~16% loss at 60°C, respectively)⁵⁰ while at this same temperature DSC devices show an up to ~60% *increase* in performance in these studies when measured at ~50-60°C after being stressed at 120°C.⁴⁶ The good stability under a wide temperature range, good low light performance, and excellent manufacturing cost projections with regard to energy payback period compared to nearly every solar cell technology⁵¹⁻⁵³ suggests DSC-based devices are excellent commercial options for specific markets including indoor lighting markets and wireless self-powered systems such as for Internet of Things (IoT) applications.^{40-41, 54}

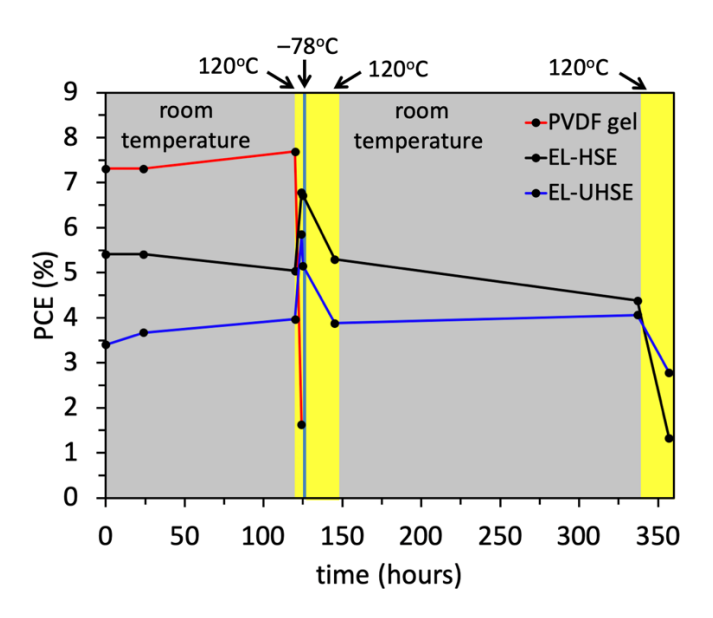


Figure 8. Device stability study using **MK2** as a sensitizer in a stand-alone DSC device under different environmental conditions.

Conclusions.

The performance of multijunction solar cell devices with bottom (third) subcells comprised of DSC, GaAs, and Si were fabricated and analyzed using DSC subcells as the first and second subcells. Using DSCs as the top and middle subcells allowed adequate photon transmission to the bottom subcell while producing significant photovoltages from early photons. Using DSC devices and Si as the bottom subcell resulted in SSM devices with higher performance than any single junction device showing a symbiotic improvement within the multijunction system. SSM-DSC devices using Black Dye as the bottom subcell gave comparable efficiencies to when GaAs was used as the bottom subcell (11.1% versus 11.2%, respectively) with photovoltage outputs in the range needed to power unbiased electrolysis of water. The DSC/DSC/GaAs device was found to perform at higher efficiencies than the device configurations using a different third subcell due to the relatively high photovoltage provided by GaAs with low energy photon use. The use of Si as the bottom subcell led to a diminished PCE value at 9.1%. Low light intensity studies reveal this is due to Si PVs operating poorly under low light conditions, such as those encountered as a bottom subcell in a multijunction stacked device. DSC devices were shown to use photons more efficiently as light intensity decreased, making them an attractive technology for multijunction systems. The exceptional performance of DSC devices under harsh environments (ranging from -78 °C to 120 °C) and reduced lighting environments such as those present in ≥3 subcell systems warrants further investigation into NIR chromophores with spectral responses at longer wavelengths than GaAs. Interestingly, DSC devices were found to increase in performance at higher temperatures which is opposite the behavior reported for many inorganic solar cells. The lack of NIR chromophores in the DSC literature efficiently using photons beyond 900 nm while retaining reasonable

photovoltages (>600 mV) is the current limiting factor for using a DSC cell as a broad absorber within multijunction systems and is the focus of future research.

EXPERIMENTAL SECTION

General Material Information. All commercially obtained reagents and solvents were used as received. Absorption spectra were measured with a Cary 5000 UV-Vis-NIR spectrophotometer. D35, Y123, and B11 were purchased from Dyenamo, Sweden. D35 was used as received. **B11** was purified with a Sephadex LH-20 column twice with methanol as eluent before use in DSCs. 55 Sephadex LH-20 was purchased from GE Healthcare Life Sciences. MK2 and **Black Dye** were purchased from Sigma-Aldrich and used as received. Co(bpy)₃^{3+/2+} and Co(bpypz)₂^{3+/2+} were prepared by following literature procedures.^{22, 32} **AP25** was prepared as previously described. ³⁶ 1H,1H,2H,2H-perfluorooctyltrimethoxysilane (PFTS) was purchased from Beantown Chemical Company. Chenodeoxycholic acid (CDCA) was purchased from Chem-Impex International. TEC 10, TEC 15 and TEC 7 were all purchased from Hartford Glass Company. Indiana, USA. Amorphous fluoropolymer CYTOP (CTL-809) and CT-Sol.180 were purchased from Asahi Glass Company, Japan. GaAs (PVM1801 GaAs BK7 K-TC, PV Measurements), Si (PVM501, PV Measurements, 7.4% PCE, used when noted), and Si (60909, Photo Emission Tech., Inc., 16.2% PCE, used unless otherwise noted) solar cells employed in this study were purchased and used as received. USA. EL-HSE and EL-UHSE utilized in the device fabrications for extreme temperature examination were purchased from Dyesol, Australia. Permabond UV6231 light curing adhesive (UV glue in the main text) was used to seal the DSC devices.

DSC Device Fabrication. *Photoanode preparation:* **D35**, **B11** and **Black Dye** DSCs were prepared as reported in the literature.^{38, 56-57} For **MK2** (second subcell), **B11** (bottom subcell) and **AP25+D35** (bottom subcell) devices, the electrodes were prepared as recently reported.^{33, 36}

Counter Electrode Preparation and Device Assembly: TEC 7 FTO glass (7 Ω /sq. sheet resistance) for bottom subcells, and TEC 15 FTO glass (15 Ω /sq. sheet resistance) for all other subcells was used to prepare the counter electrodes as previously described.³³

Preparation of CYTOP Solution and Deposition by Spin Coating: CYTOP (purchased from AGC, product number: CTL-809) was applied to both top and bottom surfaces of all DSC devices at glass-air interfaces as previously described.³³

Multijunction Device Preparation and Measurements. Once the DSC devices were fabricated as described above, copper wire leads were soldered to the FTO contacts on each device. The DSC devices were then physically stacked on top of each other in the order described for each experiment typically with a top D35 DSC device, a middle B11 device, and a varied bottom device (see Figure S9 for an image of the stack before masking and wire leads were attached). The bottom device was a DSC or inorganic solar cell. The DSC solar cells were prepared as described above, and the inorganic solar cells were purchased and used without any changes. The devices were stacked so that the photoactive areas were directly in-line (Figure S9). The stack could then either be clamped or held together with a UV curable glue. A black mask was placed over the top device so that light could only illuminate a single area, and devices below the top device received filtered light from the top device. The bottom device received light filtered by the top and middle devices only. The entire multijunction system was shielded from light on all sides except for the single illuminated opening at the top of the multijunction system. The copper wire leads were then connected in series and the multijunction solar cell efficiencies were measured via *J-V* curve

measurements exactly as a single stand-alone device is measured as described below (Figure S9). Once wired in series, the individual cells are referred to as "subcells" throughout the text to differentiate single cell measurements within the multijunction architecture and measurements on the fully wired series system. When measuring the performance of a single device within the multijunction stack, only the copper wire lead from that device were connected to the sourcemeter.

Photovoltaic Characterization. Photovoltaic characteristics were measured as previously described for single DSC devices. For series wired devices, measurements are made on the full series wired multijunction system with a single illuminated area set to 1 sun at the front device. The J-V curves are measured directly on photon-generated electricity passing through the full multijunction system. For the measurements at varied temperatures, the devices were either submerged in a dry-ice acetone bath for the time period indicated then removed and allowed to warm to around -20° C to 0° C where rapid condensation ceased to form, and the devices were then measured in front of the J-V measurement instrument. For the high temperature conditions, the devices were placed on a hot plate and covered to insulate heat for the time period indicated on the graph for the experiment. The devices were then transferred for rapid J-V measurements at a safe-to-handle temperature of 50° C to 60° C.

ASSOCIATED CONTENT

Supporting Information

Additional solution absorption data for the dyes used in these studies and additional device data are available in Electronic Supplementary Information (ESI) free of charge.

AUTHOR CONTENT

Corresponding Author

*e-mail: delcamp@olemiss.edu

Author Contributions

The manuscript was written through contributions of all authors. All authors have given approval to the final version of the manuscript. †These authors contributed equally.

ACKNOWLEDGMENTS

This research was supported by the National Science Foundation award number 1954922 with preliminary data collected under NSF award number 1455167.

REFERENCES

- 1. Butler, D., Thin Films: Ready for Their Close-Up? *Nature* **2008**, *454*, 558-559.
- 2. Polman, A.; Knight, M.; Garnett, E. C.; Ehrler, B.; Sinke, W. C., Photovoltaic Materials: Present Efficiencies and Future Challenges. *Science* **2016**, *352*, aad4424.
- 3. Jelle, B. P.; Breivik, C., The Path to the Building Integrated Photovoltaics of Tomorrow. *Energy Procedia* **2012**, *20*, 78-87.
- 4. Saifullah, M.; Gwak, J.; Yun, J. H., Comprehensive Review on Material Requirements, Present Status, and Future Prospects for Building-Integrated Semitransparent Photovoltaics (BISTPV). *J. Mater. Chem. A* **2016**, *4*, 8512-8540.
- 5. Roy, A.; Ghosh, A.; Bhandari, S.; Selvaraj, P.; Sundaram, S.; Mallick, T. K., Color Comfort Evaluation of Dye-Sensitized Solar Cell (DSSC) Based Building-Integrated Photovoltaic (BIPV) Glazing after 2 Years of Ambient Exposure. *J. Phys. Chem. C* **2019**, *123*, 23834-23837.
- 6. Luceño-Sánchez, J.; Díez-Pascual, A.; Peña Capilla, R., Materials for Photovoltaics: State of Art and Recent Developments. *Int. J. Mol. Sci.* **2019**, *20*, 976.
- 7. Ehrler, B.; Alarcón-Lladó, E.; Tabernig, S. W.; Veeken, T.; Garnett, E. C.; Polman, A., Photovoltaics Reaching for the Shockley–Queisser Limit. *ACS Energy Lett.* **2020**, *5*, 3029-3033.
- 8. NREL, National Renewable Energy Lab Best Research-Cell Efficiency Chart. https://www.nrel.gov/pv/cell-efficiency.html **2020**.
- 9. Hagfeldt, A.; Boschloo, G.; Sun, L.; Kloo, L.; Pettersson, H., Dye-Sensitized Solar Cells. *Chem. Rev.* **2010**, *110*, 6595-663.
- 10. Han, H. G.; Weerasinghe, H. C.; Min Kim, K.; Soo Kim, J.; Cheng, Y. B.; Jones, D. J.; Holmes, A. B.; Kwon, T. H., Ultrafast Fabrication of Flexible Dye-Sensitized Solar Cells by Ultrasonic Spray-Coating Technology. *Sci. Rep.* **2015**, *5*, 14645.

- 11. Fakharuddin, A.; Jose, R.; Brown, T. M.; Fabregat-Santiago, F.; Bisquert, J., A Perspective on the Production of Dye-Sensitized Solar Modules. *Energy Environ. Sci.* **2014**, *7*, 3952-3981.
- 12. Ren, Y.; Sun, D.; Cao, Y.; Tsao, H. N.; Yuan, Y.; Zakeeruddin, S. M.; Wang, P.; Gratzel, M., A Stable Blue Photosensitizer for Color Palette of Dye-Sensitized Solar Cells Reaching 12.6% Efficiency. *J. Am. Chem. Soc.* **2018**, *140*, 2405–2408.
- 13. Yoon, S.; Tak, S.; Kim, J.; Jun, Y.; Kang, K.; Park, J., Application of Transparent Dye-Sensitized Solar Cells to Building Integrated Photovoltaic Systems. *Build. Environ.* **2011**, *46*, 1899-1904.
- 14. Ahmad, S.; Guillén, E.; Kavan, L.; Grätzel, M.; Nazeeruddin, M. K., Metal Free Sensitizer and Catalyst for Dye Sensitized Solar Cells. *Energy Environ. Sci.* **2013**, *6*, 3439-3466.
- 15. Cao, Y.; Liu, Y.; Zakeeruddin, S. M.; Hagfeldt, A.; Grätzel, M., Direct Contact of Selective Charge Extraction Layers Enables High-Efficiency Molecular Photovoltaics. *Joule* **2018**, *2*, 1108-1117.
- 16. Brogdon, P.; Cheema, H.; Delcamp, J. H., Near-Infrared-Absorbing Metal-Free Organic, Porphyrin, and Phthalocyanine Sensitizers for Panchromatic Dye-Sensitized Solar Cells. *ChemSusChem* **2018**, *11*, 86-103.
- 17. Rodrigues, R. R.; Peddapuram, A.; Dorris, A. L.; Hammer, N. I.; Delcamp, J. H., Thienopyrroledione-Based Photosensitizers as Strong Photoinduced Oxidants: Oxidation of Fe(bpy)₃²⁺ in a >1.3 V Dye-Sensitized Solar Cell. *ACS Appl. Energy Mater.* **2019**, *2*, 5547-5556.
- 18. Rodrigues, R. R.; Cheema, H.; Delcamp, J. H., A High Voltage Molecular Engineered Organic Sensitizer-Iron Redox Shuttle Pair: 1.4 V DSC and 3.3 V SSM-DSC Devices. *Angew. Chem. Int. Ed.* **2018**, *57*, 5472-5476.
- 19. Kakiage, K.; Osada, H.; Aoyama, Y.; Yano, T.; Oya, K.; Iwamoto, S.; Fujisawa, J. I.; Hanaya, M., Achievement of over 1.4 V Photovoltage in a Dye-Sensitized Solar Cell by the Application of a Silyl-Anchor Coumarin Dye. *Sci. Rep.* **2016**, *6*, 35888.
- 20. Kinoshita, T.; Nonomura, K.; Joong Jeon, N.; Giordano, F.; Abate, A.; Uchida, S.; Kubo, T.; Seok, S. I.; Nazeeruddin, M. K.; Hagfeldt, A.; Grätzel, M.; Segawa, H., Spectral Splitting Photovoltaics Using Perovskite and Wideband Dye-Sensitized Solar Cells. *Nat. Commun.* **2015**, *6*, 8834.
- 21. Kang, S. H.; Jeong, M. J.; Eom, Y. K.; Choi, I. T.; Kwon, S. M.; Yoo, Y.; Kim, J.; Kwon, J.; Park, J. H.; Kim, H. K., Porphyrin Sensitizers with Donor Structural Engineering for Superior Performance Dye-Sensitized Solar Cells and Tandem Solar Cells for Water Splitting Applications. *Adv. Energy Mater.* **2016**, *7*, 1602117.
- 22. Cheema, H.; Rodrigues, R. R.; Delcamp, J. H., Sequential Series Multijunction Dye-Sensitized Solar Cells (SSM-DSCs): 4.7 Volts from a Single Illuminated Area. *Energy Environ. Sci.* **2017**, *10*, 1764-1769.
- 23. Kwon, J.; Im, M. J.; Kim, C. U.; Won, S. H.; Kang, S. B.; Kang, S. H.; Choi, I. T.; Kim, H. K.; Kim, I. H.; Park, J. H.; Choi, K. J., Two-Terminal DSSC/Silicon Tandem Solar Cells Exceeding 18% Efficiency. *Energy Environ. Sci.* **2016**, *9*, 3657-3665.
- 24. Sherman, B. D.; Bergkamp, J. J.; Brown, C. L.; Moore, A. L.; Gust, D.; Moore, T. A., A Tandem Dye-Sensitized Photoelectrochemical Cell for Light Driven Hydrogen Production. *Energy Environ. Sci.* **2016**, *9*, 1812-1817.
- 25. Eom, Y. K.; Kang, S. H.; Choi, I. T.; Yoo, Y.; Kim, J.; Kim, H. K., Significant Light Absorption Enhancement by a Single Heterocyclic Unit Change in the π -Bridge Moiety from

- Thieno[3,2-B]Benzothiophene to Thieno[3,2-B]Indole for High Performance Dye-Sensitized and Tandem Solar Cells. *J. Mater. Chem. A* **2017**, *5*, 2297-2308.
- 26. Sherman, B. D.; Sheridan, M. V.; Wee, K.-R.; Marquard, S. L.; Wang, D.; Alibabaei, L.; Ashford, D. L.; Meyer, T. J., A Dye-Sensitized Photoelectrochemical Tandem Cell for Light Driven Hydrogen Production from Water. *J. Am. Chem. Soc.* **2016**, *138*, 16745-16753.
- 27. Chae, S. Y.; Park, S. J.; Joo, O. S.; Jun, Y.; Min, B. K.; Hwang, Y. J., Highly Stable Tandem Solar Cell Monolithically Integrating Dye-Sensitized and CIGS Solar Cells. *Sci. Rep.* **2016**, *6*, 30868.
- 28. Ito, S.; Dharmadasa, I. M.; Tolan, G. J.; Roberts, J. S.; Hill, G.; Miura, H.; Yum, J. H.; Pechy, P.; Liska, P.; Comte, P.; Grätzel, M., High-Voltage (1.8V) Tandem Solar Cell System Using a GaAs/Al_xGa_(1-X)As Graded Solar Cell and Dye-Sensitised Solar Cells with Organic Dyes Having Different Absorption Spectra. *Solar Energy* **2011**, *85*, 1220-1225.
- 29. Bruder, I.; Karlsson, M.; Eickemeyer, F.; Hwang, J.; Erk, P.; Hagfeldt, A.; Weis, J.; Pschirer, N., Efficient Organic Tandem Cell Combining a Solid State Dye-Sensitized and a Vacuum Deposited Bulk Heterojunction Solar Cell. *Solar Energy Mater. Solar Cells* **2009**, *93*, 1896-1899.
- 30. Vildanova, M. F.; Nikolskaia, A. B.; Kozlov, S. S.; Shevaleevskiy, O. I.; Larina, L. L., Novel Types of Dye-Sensitized and Perovskite-Based Tandem Solar Cells with a Common Counter Electrode. *Tech. Phys. Lett.* **2018**, *44*, 126-129.
- 31. Zhang, W.; Wu, Y.; Bahng, H. W.; Cao, Y.; Yi, C.; Saygili, Y.; Luo, J.; Liu, Y.; Kavan, L.; Moser, J.-E.; Hagfeldt, A.; Tian, H.; Zakeeruddin, S. M.; Zhu, W.-H.; Grätzel, M., Comprehensive Control of Voltage Loss Enables 11.7% Efficient Solid-State Dye-Sensitized Solar Cells. *Energy Environ. Sci.* **2018**, *11*, 1779-1787.
- 32. Feldt, S. M.; Gibson, E. A.; Gabrielsson, E.; Sun, L.; Boschloo, G.; Hagfeldt, A., Design of Organic Dyes and Cobalt Polypyridine Redox Mediators for High-Efficiency Dye-Sensitized Solar Cells. *J. Am. Chem. Soc.* **2010**, *132*, 16714-16724.
- 33. Cheema, H.; Watson, J.; Delcamp, J. H., Photon Management Strategies in SSM-DSCs: Realization of a >11% PCE Device with a 2.3 V Output. *Solar Energy* **2020**, *208*, 747-752.
- 34. Chen, C.-Y.; Wang, M.; Li, J.-Y.; Pootrakulchote, N.; Alibabaei, L.; Ngoc-le, C. H.; Decoppet, J. D.; Tsai, J.-H.; Grätzel, C.; Wu, C.-G.; Zakeeruddin, S. M.; Grätzel, M., Highly Efficient Light-Harvesting Ruthenium Sensitizer for Thin-Film Dye-Sensitized Solar Cells. *ACS Nano* **2009**, *3*, 3103-3109.
- 35. Koumura, N.; Wang, Z.-S.; Mori, S.; Miyashita, M.; Suzuki, E.; Hara, K., Alkyl-Functionalized Organic Dyes for Efficient Molecular Photovoltaics. *J. Am. Chem. Soc.* **2006**, *128*, 14256-14257.
- 36. Cheema, H.; Watson, J.; Peddapuram, A.; Delcamp, J. H., A 25 mA cm⁻² Dye-Sensitized Solar Cell Based on a near-Infrared-Absorbing Organic Dye and Application of the Device in SSM-DSCs. *Chem. Commun.* **2020**, *56*, 1741-1744.
- 37. Nazeeruddin, M. K.; Péchy, P.; Renouard, T.; Zakeeruddin, S. M.; Humphry-Baker, R.; Comte, P.; Liska, P.; Cevey, L.; Costa, E.; Shklover, V.; Spiccia, L.; Deacon, G. B.; Bignozzi, C. A.; Grätzel, M., Engineering of Efficient Panchromatic Sensitizers for Nanocrystalline TiO₂-Based Solar Cells. *J. Am. Chem. Soc.* **2001**, *123*, 1613-1624.
- 38. Ozawa, H.; Awa, M.; Ono, T.; Arakawa, H., Effects of Dye-Adsorption Solvent on the Performances of the Dye-Sensitized Solar Cells Based on Black Dye. *Chem. Asian J.* **2012**, *7*, 156-62.

- 39. Luo, J.; Vermaas, D. A.; Bi, D.; Hagfeldt, A.; Smith, W. A.; Grätzel, M., Bipolar Membrane-Assisted Solar Water Splitting in Optimal pH. *Adv. Energy Mater.* **2016**, 1600100.
- 40. Freitag, M.; Teuscher, J.; Saygili, Y.; Zhang, X.; Giordano, F.; Liska, P.; Hua, J.; Zakeeruddin, S. M.; Moser, J.-E.; Grätzel, M.; Hagfeldt, A., Dye-Sensitized Solar Cells for Efficient Power Generation under Ambient Lighting. *Nat. Photon.* **2017**, *11*, 372-378.
- 41. Michaels, H.; Rinderle, M.; Freitag, R.; Benesperi, I.; Edvinsson, T.; Socher, R.; Gagliardi, A.; Freitag, M., Dye-Sensitized Solar Cells under Ambient Light Powering Machine Learning: Towards Autonomous Smart Sensors for the Internet of Things. *Chem. Sci.* **2020**, *11*, 2895-2906.
- 42. Bhagavathi Achari, M.; Elumalai, V.; Vlachopoulos, N.; Safdari, M.; Gao, J.; Gardner, J. M.; Kloo, L., A Quasi-Liquid Polymer-Based Cobalt Redox Mediator Electrolyte for Dye-Sensitized Solar Cells. *Phys. Chem. Chem. Phys.* **2013**, *15*, 17419-25.
- 43. Yadav, S. K.; Ravishankar, S.; Pescetelli, S.; Agresti, A.; Fabregat-Santiago, F.; Di Carlo, A., Stability of Dye-Sensitized Solar Cells under Extended Thermal Stress. *Phys. Chem. Chem. Phys.* **2017**, *19*, 22546-22554.
- 44. Kontos, A. G.; Stergiopoulos, T.; Likodimos, V.; Milliken, D.; Desilvesto, H.; Tulloch, G.; Falaras, P., Long-Term Thermal Stability of Liquid Dye Solar Cells. *J. Phys. Chem. C* **2013**, *117*, 8636-8646.
- 45. Jiang, N.; Sumitomo, T.; Lee, T.; Pellaroque, A.; Bellon, O.; Milliken, D.; Desilvestro, H., High Temperature Stability of Dye Solar Cells. *Solar Energy Mater. Solar Cells* **2013**, *119*, 36-50.
- 46. Sharma, K.; Sharma, V.; Sharma, S. S., Dye-Sensitized Solar Cells: Fundamentals and Current Status. *Nanoscale Res. Lett.* **2018**, *13*, 381.
- 47. Adhikari, G. C.; Thapa, S.; Zhu, H.; Zhu, P., UV Resin Enhanced Stability of Metal Halide Perovskite Nanocrystals for White Light-Emitting Diodes. *ACS Appl. Electron. Mater.* **2019**, *2*, 35-40.
- 48. Adhikari, G. C.; Zhu, H.; Vargas, P. A.; Zhu, P., UV-Green Emission from Organolead Bromide Perovskite Nanocrystals. *J. Phys. Chem. C* **2018**, *122*, 15041-15046.
- 49. Adhikari, G. C.; Vargas, P. A.; Zhu, H.; Zhu, P., Saponification Precipitation Method for CsPbBr3 Nanocrystals with Blue-Green Tunable Emission. *J. Phys. Chem. C* **2018**, *123*, 1406-1412.
- 50. Singh, P.; Ravindra, N. M., Temperature Dependence of Solar Cell Performance—an Analysis. *Solar Energy Mater. Solar Cells* **2012**, *101*, 36-45.
- 51. García-Valverde, R.; Cherni, J. A.; Urbina, A., Life Cycle Analysis of Organic Photovoltaic Technologies. *Prog. Photovolt.* **2010**, *18*, 535-558.
- 52. Ibn-Mohammed, T.; Koh, S. C. L.; Reaney, I. M.; Acquaye, A.; Schileo, G.; Mustapha, K. B.; Greenough, R., Perovskite Solar Cells: An Integrated Hybrid Lifecycle Assessment and Review in Comparison with Other Photovoltaic Technologies. *Renew. Sust. Energ. Rev.* **2017**, *80*, 1321-1344.
- 53. Greijer, H.; Karlson, L.; Lindquist, S.-E.; Hagfeldt, A., Environmental Aspects of Electricity Generation from a Nanocrystalline Dye Sensitized Solar Cell System. *Renewable Energy* **2001**, *23*, 27-39.
- 54. Khamrang, T.; Velusamy, M.; Ramesh, M.; Jhonsi, M. A.; Jaccob, M.; Ramasubramanian, K.; Kathiravan, A., IoT-Enabled Dye-Sensitized Solar Cells: An Effective Embedded Tool for Monitoring the Outdoor Device Performance. *RSC Adv.* **2020**, *10*, 35787-35791.

- 55. Cheema, H.; Islam, A.; Younts, R.; Gautam, B.; Bedja, I.; Gupta, R. K.; Han, L.; Gundogdu, K.; El-Shafei, A., More Stable and More Efficient Alternatives of Z-907: Carbazole-Based Amphiphilic Ru(II) Sensitizers for Dye-Sensitized Solar Cells. *Phys. Chem. Chem. Phys.* **2014**, *16*, 27078-87.
- 56. Cheema, H.; Delcamp, J. H., Harnessing Photovoltage: Effects of Film Thickness, TiO₂ Nanoparticle Size, MgO and Surface Capping with DSCs. *ACS Appl. Mater. Interfaces* **2017**, *9*, 3050-3059.
- 57. Cheema, H.; Delcamp, J. H., The Role of Antireflective Coating CYTOP, Immersion Oil, and Sensitizer Selection in Fabricating a 2.3 V, 10% Power Conversion Efficiency SSM-DSC Device. *Adv. Energy Mater.* **2019**, *9*, 1900162.
- 58. Cheema, H.; Delcamp, J. H., SnO₂ Transparent Printing Pastes from Powders for Photon Conversion in SnO₂ -Based Dye-Sensitized Solar Cells. *Chem. Eur. J.* **2019**, *25*, 14205-14213.

ABSTRACT GRAPHIC

